Fizika Nizkikh Temperatur, 2005, v. 31, Nos. 3/4, p. 412–421

Pressure effect on the Fermi surface and electronic structure of $LuGa_3$ and $TmGa_3$

V.B. Pluzhnikov

International Laboratory of High Magnetic Fields and Low Temperatures
Gajowicka 95, 53-529 Wrocław, Poland
B. Verkin Institute for Low Temperature Physics and Engineering
of the National Academy of Sciences of Ukraine, 47 Lenin Ave., Kharkov 61103, Ukraine

G.E. Grechnev

B. Verkin Institute for Low Temperature Physics and Engineering
of the National Academy of Sciences of Ukraine, 47 Lenin Ave., Kharkov 61103, Ukraine
E-mail: grechnev@ilt.kharkov.ua

A. Czopnik

W. Trzebiatowski Institute of Low Temperature and Structure Research
P.O. Box 1410, 50-950 Wrocław, Poland

O. Eriksson

Theoretical Magnetism Group, Department of Physics, University of Uppsala
Box 530, S-751 21 Uppsala, Sweden

Received August 31, 2004

The Fermi surfaces and cyclotron masses of $LuGa_3$ and $TmGa_3$ compounds are studied by means of the de Haas–van Alphen effect technique under pressure. The highly anisotropic pressure dependences of the de Haas–van Alphen frequencies and cyclotron masses have been observed in both compounds. Concurrently, the *ab initio* calculations of the volume-dependent band structures have been carried out for these compounds, including ferromagnetic configuration phase of $TmGa_3$, by employing a relativistic version of the full-potential linear muffin-tin orbital method within the local spin-density approximation. The experimental data have been analysed on the basis of the calculated volume-dependent band structures and compared with the corresponding pressure effects in the isostructural compound $ErGa_3$.

PACS: **71.18.+y**, 71.20.Eh, 71.70.Gm

1. Introduction

In the recent years the de Haas–van Alphen effect (dHvA) has been extensively studied in a number of RM_3 compounds (R is a rare-earth, M is a *p* element from the group-III series), including RGa_3 [1–4], light RIn_3 (R = La – Gd) [5], heavy RIn_3 (R = Tb – Lu) [6], $TmAl_3$ [7], and $CeIn_3$ [8]. The main objective of these studies was to determine the Fermi surface (FS) geometry and effective cyclotron masses in the representative series of RM_3 compounds. The role of magnetic ordering in reconstruction of the FS has been also addressed in Refs. [5,6] (RIn_3), [9] ($TmGa_3$), and [10] ($ErGa_3$).

In the present work we study the effect of pressure on the FS and cyclotron masses of the $LuGa_3$ and $TmGa_3$ compounds by means of the dHvA effect. The pressure derivatives of dHvA frequencies and cyclotron masses are of particular interest due to their sensitivity to details of the exchange interaction and many-body effects in R systems. Therefore, the present investigation can provide a critical test for recently developed methods of *ab initio* calculations of electronic and magnetic structures, and to stimulate

the formulation of improved theories for electronic structure of rare earths.

This work represents an extension of our recent studies [1–3] of the FS and electronic structure in RGa_3 compounds at ambient pressure. Also, the pressure effect on the FS of $ErGa_3$ has been addressed in Ref. 4. Information on physical properties of $TmGa_3$ and $LuGa_3$ is scarce. These compounds crystallize in the $AuCu_3$-type cubic structure. At T_N = 4.26 K $TmGa_3$ orders antiferromagnetically [11] to the multiaxial 3**k**-type magnetic structure [12,13]. It has been shown [14], that in the paramagnetic state an interaction between quadrupolar moments of the 4*f* shells is strong, and it leads to their ordering just above T_N, and the leading mechanism appears to be the pair quadrupolar interaction via conduction electrons.

It can be expected that at low temperatures $TmGa_3$ reveals large and field-dependent magnetization, in the same manner as is the case of $ErGa_3$ [3,4]. It brings about, as in the case of $ErGa_3$ [4], a number of difficulties in the Fourier analysis of dHvA oscillations. As a result, one has to study the dHvA effect in strong enough magnetic fields where magnetization tends to saturate. Obviously, these fields are required to be higher than the critical field destroying the antiferromagnetic order. Therefore, the dHvA effect can be studied in a paramagnetic phase of $TmGa_3$, in which sufficient magnetic fields lead to a quasi-ferromagnetic configuration of magnetic moments.

In this work, the experimental investigation of the dHvA effect under pressure is supplemented by *ab initio* calculations of the volume-dependent electronic structures of $TmGa_3$ and the reference compound $LuGa_3$. This provides the possibility of estimating many-body enhancement of «bare» cyclotron masses, and the mass enhancement factors λ can be evaluated with the observed (m_c^*) and calculated (m_c^b) cyclotron masses.

Also, a comparison of the dHvA data under pressure and the calculated volume-dependent band structures is expected to be very useful for development of advanced theoretical models for electronic spectra of rare-earth compounds. The evaluated parameters of the electronic structure of $TmGa_3$ and $LuGa_3$ and their pressure derivatives are compared with the corresponding results obtained for the isostructural $ErGa_3$ compound at high pressures [4]. This comparison provides the possibility of estimating the anisotropy and volume dependences of the FS and the many-body enhancement of the cyclotron masses in heavy RGa_3 rare-earth compounds.

A discussion is given on the role of different interactions (exchange splitting, magnetic quadrupolar excitations, spin waves, crystal field) in the revealed pressure effects on the FS and cyclotron masses.

2. Experimental details

Single crystals of $TmGa_3$ and $LuGa_3$ were grown by the flux method from a melt of the nominal composition 90 at.% Ga and 10 at.% Tm or Lu. The purity of starting metals was 6N for Ga and 4N for Tm and Lu. The feed placed in an alumina crucible and sealed in a quartz tube in an argon atmosphere under a pressure of 150 Torr at room temperature, was heated in a resistance furnace up to 920 °C, held at this temperature for 48 h and then slowly cooled down at the rate 0.8 K/h. The synthesis was stopped at about 350 °C and then sample was cooled fast down to room temperature to avoid the formation of RGa_6 in a peritectic reaction [15]. The resulting crystals of $TmGa_3$ and $LuGa_3$ were immersed in an excess of Ga which is easy to remove. The crystals obtained had the form of cubes with maximum dimensions 5×5×5 mm. According to an x-ray examination the quality of the single crystals was very good.

The magnetic phase diagram of $TmGa_3$ in magnetic field parallel to the ⟨100⟩ axis is shown in Fig. 1 (cited from Ref. 13). The antiferroquadrupolar phase exists only in low fields up to 0.5 T and in the very narrow range of temperatures: $(T_Q - T_N) < 0.1$ K. The critical lines $H_{c1}(T)$ and $H_{c2}(T)$ are the lines of metamagnetic transitions: at the field $H_{c1}(T)$ from the 3**k** phase to an intermediate one and at $H_{c2}(T)$ from the intermediate phase to a paramagnetic one. In a field applied along the other two principal crystallographic axes, ⟨110⟩ and ⟨111⟩, the phase diagrams are similar to that cited, but the critical field $H_{c2}(T)$ reaches much lower values and does not exceed 2.2 T [13]. At temperatures lower than T_N and in magnetic field higher than 7 T, magnetic moments reach an induced paramagnetic configuration, except for a small region of angles at the ⟨100⟩ axis. Above the second metamagnetic transition the magnetization is large and anisotropic. This fact has important consequences for analysis of the dHvA effect in $TmGa_3$.

First, in the Fourier analysis of the dHvA signal $V_{\rm osc}$ one must take into account the magnetic induction B in the Lifshitz–Kosevich formula instead of the applied magnetic field $H_{\rm appl}$,

$$V_{\rm osc} \approx A \sin\left[\left(\frac{2\pi F}{B}\right) + \varphi\right], \qquad (1)$$

where the dHvA frequency F is proportional to the extremal cross-sectional area of the FS, and the magnetic induction $B = H_{\rm appl} + 4M(1 - N)$ depends on

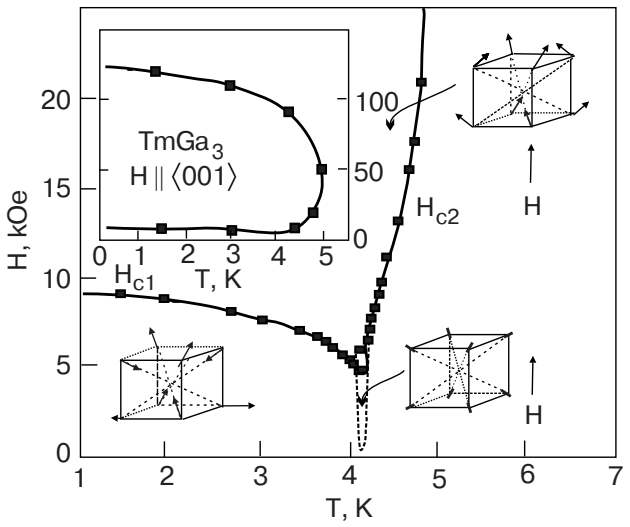

Fig. 1. Low-field magnetic phase diagram of $TmGa_3$ in magnetic field applied along the ⟨001⟩ axis (cited from Ref. 13). The inset shows the whole diagram.

the magnetization per unit volume M and on the demagnetizing factor N.

Secondly, the cyclotron effective mass, m_c^*, is determined from the temperature dependence of the dHvA amplitude A, namely, from the slope of the plot of $\ln \{A[1 - \exp(-2\alpha m_c^* T/B)]/T\}$ versus T, where $\alpha = 2\pi^2 c k_B/e\hbar$. Therefore, one has to take into account the magnetic induction B instead of the applied magnetic field H_{appl}.

Thirdly, in a strong magnetic field the magnetic moments of Tm^{3+} ions reach spin-polarized paramagnetic configuration. Then the k–f exchange interaction leads to a splitting of the conduction band into sub-bands, and the value of this band splitting is proportional to the magnetic moment, density of states, and the k–f exchange integral.

The dHvA effect measurements for the magnetic $TmGa_3$ were performed on a spherical sample (diameter 2.5 mm) by using a standard field modulation technique at temperatures down to 1.5 K and in magnetic fields up to 13 T applied along the principal crystallographic axes. For a spherical sample, as we have used, one has $B = H_{\text{appl}} + (8\pi/3)M$. The magnetization in magnetic fields, used for the dHvA effect study, depends rather weakly on the magnetic field strength. Complementary magnetization measurements were performed by a home-made vibrating sample magnetometer.

A standard Cu–Be clamp was used for the pressure effect study with an extracted benzine solvent as the medium transmitting pressure to the sample. The maximum pressure employed was 6.4 kbar at 4.2 K. A small Manganin coil with resistance about 60 Ω was placed near the sample to measure the applied pressure. Preliminarily this coil had been trained to cooling-pressure and then calibrated by measuring the superconducting transition temperature of Sn [16]. The deviation of the Manganin coil resistance due to the residual magnetic field of the superconducting magnet has been also taken into account. The sample, the pick-up coil, and the Manganin coil, all were placed in a Teflon cell, filled with the extracted benzine solvent, and then the cell was put into the pressure clamp. The deviation from hydrostatic pressure and its effect on the measurements are estimated to be negligible by observing that the superconducting transition width of Sn does not change noticeably, and the amplitudes of the dHvA oscillations do not decrease substantially under the pressures used in this work. Since the pressure clamp is heated by the modulation field, there is a difference in temperatures between the helium bath and the sample in the pressure clamp. The modulation amplitude and frequency used in the measurements were 40 G and 38.5 Hz, respectively. These amplitude and frequency were chosen to produce a large enough dHvA signal, and, at the same time, to reduce the heating power, which leads to a temperature difference not exceeding 0.02 K.

The applied pressure modifies the magnitude and field dependence of the magnetization due to a pressure effect on the crystal field (CF) splitting, as well as on the exchange interaction [2,3]. It is known that the CF of metallic rare-earth compounds contains contributions from charges of surrounding ligands as well as from the direct Coulomb and exchange interactions of the R ion with conduction electrons. In order to estimate the influence of pressure on the CF we have restricted ourselves to the contribution from surrounding ligands within the point charge model. The applied pressure P brings about the volume dilatation $\delta V/V = -P/c_B$, were c_B is the bulk modulus. Under a pressure of 10 kbar $\delta V/V$ is estimated to be −0.013, provided the bulk modulus of $TmGa_3$ is taken from Ref. 14 (c_B = 765 kbar). The change of CF due to this dilatation causes a variation of the magnetic induction not larger than 20 G at 1.7 K in an applied field of 13 T. One can also estimate the change of the magnetization in $TmGa_3$ due to the variation of the exchange interaction parameter under pressure by using the data obtained for the isostructural RIn_3 compounds [17,18]. The corresponding variation of the magnetic induction at an applied pressure of 10 kbar is about −10 G at 1.7 K in a field of 15 T. Therefore, the total change of the magnetic induction reaches only 10 G, giving a relative variation of the dHvA frequency $\delta F/F \approx 2 \cdot 10^{-4}$ kbar^{-1}, which can be neglected in the Fourier analysis of the dHvA oscillations.

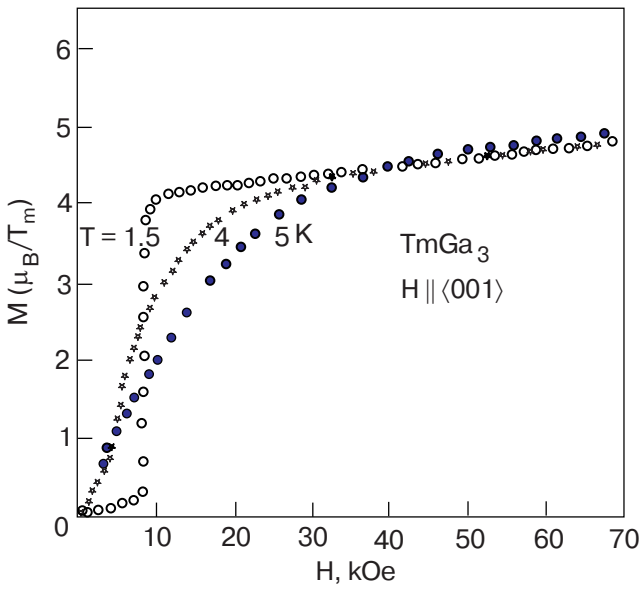

Fig. 2. Magnetization of $TmGa_3$ in the magnetic field applied along ⟨001⟩ at different temperatures (cited from Ref. 13).

The dHvA effect measurements were carried out in magnetic fields higher than 7 T, where the magnetization does not change appreciably and the Fourier analysis of the dHvA oscillations can be performed. Otherwise a dHvA frequency would change its value following the strength of external magnetic field. Therefore, the dHvA effect studies were carried out in the paramagnetic phase well above the $H_{c2}(T)$ line of the antiferromagnetic–paramagnetic transition (Fig. 1), except for the ⟨100⟩ axis, for which the critical field reaches significant values. The magnetization in magnetic fields higher than 7 T tends to saturate, and the magnetic moments settle into a quasi-ferromagnetic configuration. Moreover, the magnetization along all directions in a magnetic field higher than 7 T appeared to be almost temperature independent in the range 1.7–4.2 K (Fig. 2, cited from Ref. 13).

The effects of the antiferromagnetic and antiferroquadrupolar order on the FS of $TmGa_3$ have not been examined in this study. For these phases the large magnetization value and its strong dependence on magnetic field have not allowed analysis of the dHvA oscillations. Also, a very narrow temperature range (< 0.1 K) for the antiferroquadrupolar phase has prevented the corresponding study of the dHvA effect.

3. Details of calculations

A treatment of localized strongly correlated 4*f* electrons still presents a challenge to the band structure theory. The results of *ab initio* calculations (see, e.g., Refs. [2,3,18–21]) together with a wealth of experimental data (including bulk and FS properties) provide solid evidence that within the local spin-density approximation (LSDA) [22] a strict band treatment of the 4*f* states is inadequate for heavy rare earths. The *f* shell is not filled, and the 4*f* bands, which act as a sink for electrons, would always cut the Fermi level E_F leading to absurd values of the specific heat coefficients [19] and wrong 4*f* occupancies, close to the divalent (i.e., atomic) configuration [23].

According to the photoemission data [23–25], the 4*f* spectral density for Er, Tm, and their compounds were observed about 5 eV below E_F. Therefore, in order to describe the band structure of the ground state of $TmGa_3$ near E_F, it is feasible to consider the 4*f* states as semi-localized core states, in line with Refs. [18,20,26]. The bulk and magnetic properties calculated within this approach, as well as the Fermi surfaces of Gd, Tb [20], and ErAs [21] appeared to be in agreement with experimental data. Actually, the standard rare-earth model [19] is employed in this work in the limit of large Hubbard repulsion U within the *ab initio* LSDA scheme [22] for the exchange-correlation effects. The localized *f* states of Tm were treated as spin-polarized outer-core wave functions, contributing to the total spin density, and the spin occupation numbers were fixed by applying the Russel–Saunders coupling scheme to the 4*f* shell, which was not allowed to hybridize with conduction electrons.

The *ab initio* band structure calculations were carried out for the paramagnetic configuration phase of$TmGa_3$ and non-spin-polarized $LuGa_3$ by using the full potential linear muffin-tin orbital method (FP-LMTO) [27,28]. In the case of $TmGa_3$, the spin density of the 4*f* states polarizes the «spin-up» and «spin-down» conduction electron states through the local exchange interaction. The exchange split conduction electron states interact with the localized *f* states at other sites, appearing as the medium for the indirect *f*–*f* interaction [18,26]. In order to calculate FS orbits for both $TmGa_3$ and $LuGa_3$, the charge densities were obtained by including spin-orbit coupling at each variational step, as suggested in Refs. [19,20]. The band structures and crystal potentials were calculated self-consistently on a uniform mesh of 455 **k** points in the irreducible wedge of the cubic Brillouin zone for a number of lattice parameters close to the experimental ones (a = 4.196 Å and 4.180 Å for $TmGa_3$ and $LuGa_3$, respectively). The bulk moduli c_B were evaluated from the calculated total energies $E(V)$ as functions of volume V (i.e., from the theoretical equations of states, according to Ref. 27), and were estimated to be about 800 kbar for $TmGa_3$ and $LuGa_3$, which is close to the experimental value c_B = 765 kbar ($TmGa_3$ [14]). This is a rather normal overestimation

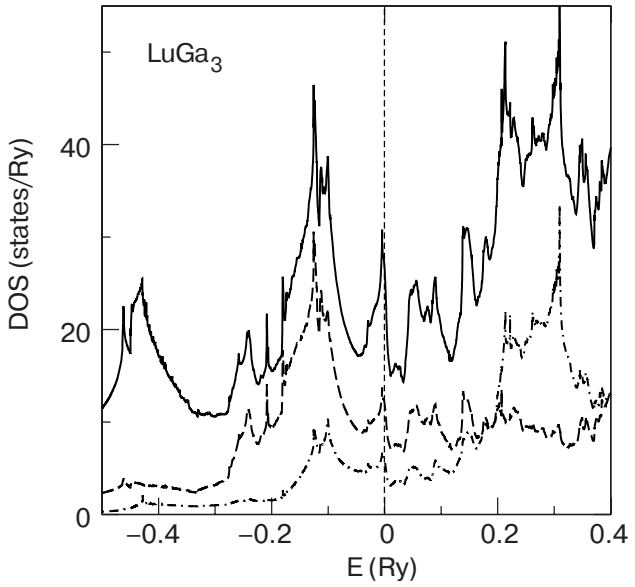

Fig. 3. Total (solid line) and partial densities of states (DOS) $N(E)$ relative to the Fermi energy $E_F = 0$ for $LuGa_3$. The dashed line stands for the p states of Ga, and the dashed-dotted line represents d states of Lu.

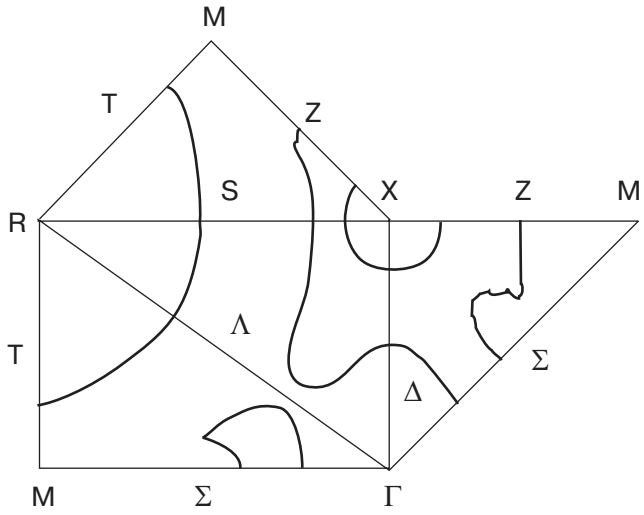

Fig. 4. Intersection of the Fermi surface for $LuGa_3$ with the Brillouin zone faces.

of c_B, presumably due to the overbonding tendency of LSDA.

The calculated total and partial densities of states (DOS) $N(E)$ for $LuGa_3$ are presented in Fig. 3. There are two fairly broad peaks (bonding and antibonding states) arising due to hybridization of 5d states of Lu and the p states of Ga. As can be seen in Fig. 3, these p states give a substantial contribution to the conspicuous peak in the total DOS at the Fermi energy E_F. The calculated total and partial DOS for $TmGa_3$ appeared to be in a qualitative agreement with the $N(E)$ of $LuGa_3$, as well as with the previously calculated $TmGa_3$ DOS (see Fig. 7 in Ref. 2). The intersections of the calculated FS of $LuGa_3$ with faces of the cubic Brillouin zone (Fig. 4) show the almost spherical electron FS centered at the R point and the complicated multiply connected hole FS centered at the Γ and X points, analogously to $TmGa_3$ and also $ErGa_3$ ([3]). As a whole, the electron FS of RGa_3 is nearly spherical, whereas the hole FS is a complicated multiply connected surface.

In agreement with the results of Ref. 20 for Gd and Tb, the incorporation of the spin–orbit coupling has a small effect on the calculated dHvA frequencies and cyclotron masses. It should be noted that for the field-induced quasi-ferromagnetic configuration of $TmGa_3$ the exchange splitting is larger than the spin–orbit splitting, and the dHvA spectrum of $TmGa_3$ can be compared with the results of band structure calculations for the spin-polarized state.

4. Results and discussion

The Fourier spectra of dHvA oscillations in $TmGa_3$, observed along ⟨100⟩ axis at different pressures, are presented in Fig. 5, and the pressure effect on the corresponding dHvA frequencies is exhibited in Fig. 6. The branch a originates from the belly orbit in the band 7 electron FS centered at the R point, whereas the d orbit comes from the nearly spherical

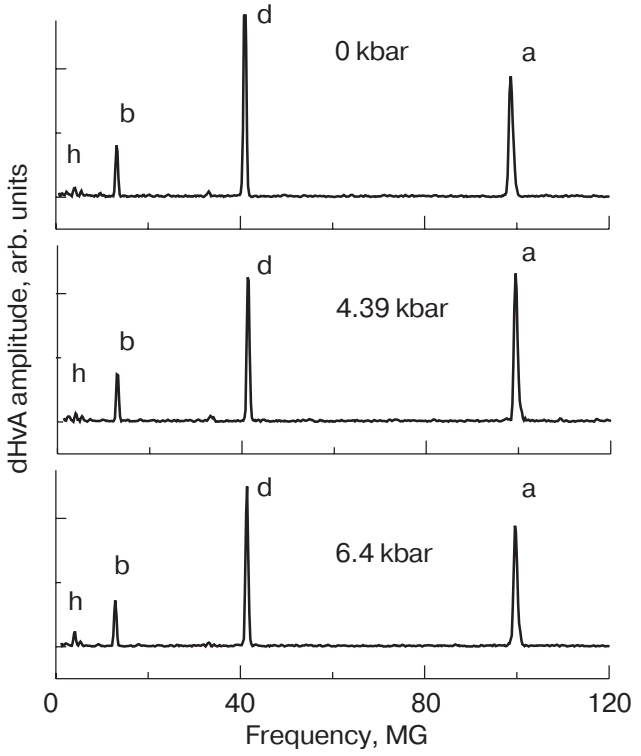

Fig. 5. Fourier spectra of the dHvA oscillations observed in $TmGa_3$ at 1.9 K for magnetic fields directed along ⟨001⟩ axis at different pressure.

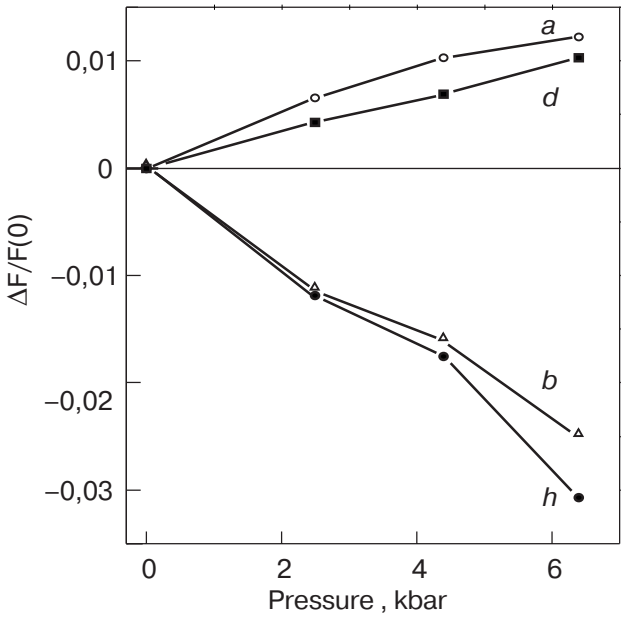

Fig. 6. Fractional changes of the dHvA frequencies, $\Delta F/F(0) = [F(P) - F(0)]/F(0)$, in $TmGa_3$ as a function of pressure for the ⟨001⟩ magnetic field direction at 1.9 K. The frequencies are labeled according to Ref. 2 and Fig. 5. The solid lines are guides for the eye.

part of the hole FS at the Γ point (see Fig. 4). The orbit *b* is associated with the FS centered at the X point, and the low frequency orbits *h* are related to «arms» in the band 6 hole FS. At ambient pressure the experimental angular dependent dHvA frequencies appeared to be very close to those previously reported for $TmGa_3$ and $LuGa_3$ (Figs. 2 and 3 in Ref. 2, respectively), and also to the results of the present FP-LMTO calculations.

In the range of high dHvA frequencies (branches *a* and *d*) the spectra of $LuGa_3$ and $TmGa_3$ are very similar. In the low dHvA frequency range, instead of single *b* and *h* branches for $LuGa_3$, two *b* and several *h*-type branches were observed for $TmGa_3$. For all principal crystallographic axes, ⟨100⟩, ⟨110⟩, and ⟨111⟩, the dHvA frequencies F at ambient pressure, their pressure derivatives, $d\ln F/dP$, the corresponding cyclotron masses m_c^* together with their pressure derivatives, $d\ln m_c^*/dP$, are given in Tables 1 and 2 for $LuGa_3$ and $TmGa_3$, respectively. The pressure coefficients $d\ln F/dP$ are determined by fitting a straight line to each set of data in $\ln F$ versus P plots (see, e.g., Fig. 6). For comparison and further discussion, the analogous results on F, $d\ln F/dP$, and m_c^* in the isovalent $ErGa_3$ compound are taken from our paper [4] and shown in Table 3. It is worth noting that the «exchange-split» dHvA oscillations, which should originate from the slightly spin-polarized sub-bands of $TmGa_3$, were not resolved in this work within the limits of the large experimental errors. In contrast to investigations of Refs. [2,3], in the present dHvA experiments additional errors emerged due to the weak signal from the pick-up coil, which had to be placed in the pressure clamp, and also due to possible non-hydrostatic pressure conditions at the sample. Therefore, only solid and reliable high pressure results are presented in the Tables, whereas questionable data are omitted.

Table 1. The dHvA frequencies F (in MG) and the corresponding cyclotron effective masses m_c^* (in units of free electron mass) in $LuGa_3$ at ambient pressure, their logarithmic pressure derivatives (in 10^3 kbar^{-1}), and the mass enhancement factor λ.

Field direction, branch	F	$d\ln F/dP$		m_c^*		λ	$d\ln m_c^*/dP$	
	exper.	exper.	theory	exper.	theory		exper.	theory
⟨100⟩, *a*	98.06	+1.2(0.2)	1.0	0.74	0.38	0.95	—	—
d	41.3	+1.0(0.2)	1.3	0.63	0.48	0.31	−15(3)	−5
b	11.87	−3.4(0.1)	—	0.3	—	—	−6.5(0.3)	—
h	4.92	—	—	0.33	—	—	−38(9)	—
⟨110⟩, *a*	94.6	+1.2(0.2)	0.9	0.73	0.36	1.03	—	—
b′	14.9	−2.6(0.2)	—	0.36	—	—	+17(3)	—
b	12.76	−3.0(0.2)	—	0.47	—	—	+12(2)	—
h	3.97	−4.2(0.4)	—	0.23	—	—	+35(1)	—
⟨111⟩, *a*	88.6	+1.3(0.8)	1.0	0.57	0.36	0.58	−8.5(1)	−3
d	35.6	+1.6(0.2)	1.4	0.53	0.39	0.36	−5.5(2)	−4
h	4.8	−3.1(0.6)	–	0.24	—	—	−20(1)	–

Table 2. The dHvA frequencies F (in MG) and the corresponding cyclotron effective masses m_c^* (in units of free electron mass) in $TmGa_3$ at ambient pressure, their logarithmic pressure derivatives (in 10^3 kbar^{-1}), and the mass enhancement factor λ.

Field direct-ion, branch	F	$d \ln F / dP$		m_c^*		λ	$d \ln m_c^* / dP$	
	exper.	exper.	theory	exper.	theory		exper.	theory
⟨100⟩, a	98.68	+1.8(0.3)	1.2	1.24	0.41	2.0	+1.6(1.6)	−4
d	41.1	+2.0(0.4)	1.6	1.3	0.46	1.8	−14(3)	−7
b	11.61	−3.8(0.2)	–	0.83	–	–	+16(8)	–
h	3.58	−4.5(1.7)	–	–	–	–	–	–
⟨110⟩, a	94.41	+1.5(0.1)	1.1	1.04	0.38	1.7	−7(4)	−4
b'	14.46	−2.9(0.3)	–	–	–	–	–	–
b	12.66	−2.8(0.1)	–	0.96	–	–	−29(6)	–
h'	4.8	−2.3(0.2)	–	–	–	–	–	–
h	3.57	−4.3(0.3)	–	0.46	–	–	–	–
⟨111⟩, a	87.28	+1.8(0.3)	1.1	0.91	0.38	1.4	+22(10)	−3
d	34.24	+2.1(0.5)	1.5	0.83	0.42	1.0	+3.6(0.7)	−6
h	4.31	−6.0(0.3)	–	0.46	–	–	−22(6)	–

Table 3. The dHvA frequencies F (in MG) at ambient pressure, their logarithmic pressure derivatives (in 10^3 kbar^{-1}), the corresponding cyclotron effective masses m_c^* (in units of free electron mass), and the mass enhancement factor λ in $ErGa_3$ compound.

Field direct-ion, branch	F	$d \ln F/dP$		m_c^*		λ
	exper.	exper.	theory	exper.	theory	
⟨100⟩, a	98.71	+2.3(0.3)	1.3	0.96	0.40	1.4
d	41.07	+1.7(0.2)	2.0	0.91	0.46	0.98
b	12.66	−2.7(0.1)	− 2.8	0.44	–	–
h	4.35	–	–	0.55	–	–
⟨110⟩, a	95.17	+1.0(0.3)	1.1	0.89	0.37	1.4
b'	15.14	−1.1(0.1)	–	0.57	–	–
b	11.95	−2.4(0.2)	−2.0	0.84	–	–
h	3.37	−4.5(0.3)	–	0.28	–	–
⟨111⟩, a	87.58	+1.7(0.1)	1.2	0.80	0.37	1.16
d	35.47	+2.3(0.2)	1.9	0.70	0.40	0.75
h	4.21	–	–	0.51	–	–

As is seen from the Tables, the larger dHvA frequencies a and d increase with pressure. On the other hand, for the hole FSs b and h the derivatives $d \ln F/dP$ appeared to be negative. Also, the observed pressure dependences of the dHvA frequencies are quite different among $ErGa_3$, $TmGa_3$, and the non-f reference compound $LuGa_3$. The experimental pressure derivatives $d \ln F/dP$, presented in Tables 1 and 2, are rather large in comparison with the free-electron scaling prediction, which gives two-thirds of the volume compressibility, or $0.87 \cdot 10^{-3}$ kbar^{-1}, provided the available bulk modulus of $TmGa_3$ [14] is accepted. This scaling estimation actually means that with increasing pressure, the volumes of the Brillouin

zone and the FS increase, and one can also expect that both the hole and electron FS increase. However, this effect cannot explain the negative pressure derivatives for the hole FS.

In the framework of the band theory, the overlap of the wave functions between the $4p$ bands of Ga and the $5d$ bands of R increases with pressure, and the $p-d$ hybridization becomes stronger. Consequently, while the volume of the big spherical FS sheets increases, the volumes of small «arms» of the hole FS may decreases due to strong hybridization and substantial deviation from free-electron scaling, and this can provide the anisotropic dHvA frequency changes. Basically, there is qualitative agreement between the experimental and calculated derivatives $d\ln F/dP$ for the a and d orbits in $LuGa_3$ (again, the bulk modulus of $TmGa_3$ was used to convert the calculated volume derivatives to the pressure ones, listed in the Tables). However, this band approach can not explain the discrepancy between the experimental and calculated pressure derivatives of the dHvA frequencies in $TmGa_3$.

It was originally suggested in Ref. 29, that in ferromagnetic systems there are two contributions to the pressure derivative of a dHvA frequency. The first («potential») contribution comes from an atomic volume effect on the crystal potential, and also from a scaling effect due to the change of the Brillouin zone size. It can be approximated by the corresponding derivative for a nonmagnetic reference compound with a close value of the compressibility (in our case it can be $LuGa_3$). The second («magnetic») contribution originates from the pressure induced redistribution of conduction electrons between exchange-split sub-bands and the corresponding changes of the volume enclosed by the FS sheets. According to the present calculations, the Fermi surfaces of $TmGa_3$ do not change uniformly because of a strong **k**-dependent $p-d$ mixing effect on the exchange-split conduction band. As a result, the difference between pressure derivatives of the spin-split FS cross-sectional areas is inconsistent with simple estimations based on the Stoner–Wohlfarth model.

Glancing at the experimental lattice parameters, which are very close in $TmGa_3$ and $LuGa_3$, one may assume that crystal potential in the two compounds does not differ substantially, and that the differences in the dHvA frequencies derivatives of $TmGa_3$ and $LuGa_3$ compounds can be attributed to the unfilled $4f$ shell in $TmGa_3$. In the $4f$ spin-polarized state the differences can arise, first, from the exchange splitting of the conduction band of $TmGa_3$, and, secondly, from the magnetostriction effects due to the $\Gamma_5^{(1)}$ CF ground state of the $^3H_6$ multiplet of Tm^{3+} ion. Unfortunately, at the present stage the differences in $d\ln F/dP$ can not be ascribed confidently either to the conduction band splitting or to the magnetostriction.

Cyclotron masses m_c^* have been determined at ambient and high pressures for the most dHvA frequencies in the field applied along the ⟨100⟩, ⟨110⟩, and ⟨111⟩ axes, and are presented in Tables 1 and 2. Band cyclotron masses m_c^b were calculated for the a and d branches, and were also given in the Tables. Also, the cyclotron masses measured and calculated for $ErGa_3$ in Refs. [3,4] are listed in Table 3 for comparison.

The mass enhancement factor λ, which is defined by relation $m_c^* = m_c^b(1+\lambda)$, presents a measure of the interaction strength of the conduction electrons with low-energy excitations, and it can be determined by comparison of the experimental cyclotron effective masses with the corresponding calculated ones. The λ factors for electrons on the a and d orbits in $LuGa_3$, $TmGa_3$, and $ErGa_3$ are listed in the Tables. In the nonmagnetic $LuGa_3$ the λ factor represents a measure of the electron–phonon interaction, whereas in $ErGa_3$ and $TmGa_3$ this factor also contains contribution(s) coming from magnetic excitations. As seen in Table 1, in $LuGa_3$ the λ factor ranges from 0.3 (d branch) to about 1 (a branch). Assuming that the values of $\lambda_{e\text{-ph}}$ in RGa_3 are close to the corresponding ones in $LuGa_3$, we estimated the magnetic contributions λ_{mag} in $ErGa_3$ to be 0.4–0.6 and 0.4–0.7 for the a and d orbits, respectively. In $TmGa_3$ the corresponding values of λ_{mag} are larger and more anisotropic, namely, 0.5–1 and 0.8–1.5.

The hybridization of conduction electrons with $4f$ states could contribute to the larger cyclotron masses observed in $TmGa_3$ and $ErGa_3$ as compared to $LuGa_3$. However, a strong hybridization with $4f$ bands in the framework of the LSDA would lead to a substantial reduction of the conduction band width in RGa_3 and thus to bulk properties remarkably different from that in $LuGa_3$. In fact, the lattice parameters decrease slightly in a linear fashion in the series $ErGa_3$, $TmGa_3$, and $LuGa_3$ due to the lanthanide contraction, and it can be expected that conduction band widths are close in RGA_3, and therefore band cyclotron masses should be also close. At the present stage more elaborated analysis is necessary to estimate the scale of the hybridization effects by employing modern theoretical schemes (like the LSDA + U approach) and additional experimental data (e.g., for related RIn_3 compounds).

One can also assume that the distinctions between effective masses in RGa_3 are probably due to the different ground state multiplets $^3H_6$ and $^4I_{15/2}$ of Tm^{3+} and Er^{3+} ions in the CF of $TmGa_3$ and $ErGa_3$, respectively. The triplet $\Gamma_5^{(1)}$ with intrinsic magnetic

and quadrupolar moments is the ground state in $TmGa_3$ [14], and most likely Γ_7 is the ground state in CF of $ErGa_3$ [30]. Since the $\Gamma_5^{(1)}$ state exhibits quadrupolar moment and the Γ_7 state does not, one can expect large magnetostriction effects in $TmGa_3$ and none in $ErGa_3$.

In this connection one can expect that the presence of strong quadrupolar interactions increases the cyclotron effective masses. It is well known [31] that the quadrupolar excitations does not occur in compounds with the cubic symmetry. They may appear, however, in $TmGa_3$ as coupled magnetic-quadrupolar excitations in applied magnetic field [14]. It was shown in Ref. 31 that the corresponding excitations contribute to the effective mass of the conduction electrons, and the effect appears to be large and magnetic field dependent. Also, in the quasi-ferromagnetic configuration of magnetic moments, the exchange splitting of the conduction bands can vary in $ErGa_3$ and $TmGa_3$ due to the difference in corresponding $4f$-shell spin occupation numbers. At the moment, however, one can not estimate the relative contributions of the conduction band splitting and the magnetostriction to the observed differences in cyclotron masses and the pressure dependences of the dHvA frequencies in $TmGa_3$ and $ErGa_3$.

Also, one more mechanism can affect the cyclotron masses in RGa_3. It was shown in Refs. [31–33] that virtual magnetic excitations can contribute substantially to the effective mass of the conduction electrons in rare-earth systems. These excitations are magnetic excitons in a paramagnetic system (e.g., praseodymium), and spin waves in magnetically ordered rare earths. The corresponding mass enhancement is expected to be large, magnetic field dependent, and proportional to the static susceptibility of the magnetic system. According to estimations of the electronic specific-heat coefficients in Ref. 33, the corresponding effective masses increase in the series of heavy rare-earth metals. This trend is consistent with the relation between observed cyclotron masses in $ErGa_3$ and $TmGa_3$, and also in $ErIn_3$ and $TmIn_3$ compounds [6]. However, considerable work is needed to implement findings of Refs. [32,33] for a quantitative description of cyclotron masses in magnetic RM_3 compounds.

In conclusion it should be noted that the calculated LSDA band cyclotron masses m_c^b did not reproduce the highly anisotropic pressure derivatives of m_c^* in $TmGa_3$ (see Table 2), which are presumably determined by various magnetic and many-body excitations. On the other hand, the calculated $d\ln m_c^b/dP$ in $LuGa_3$ appeared to be in a qualitative agreement with the corresponding experimental data in Table 1.

Summary

As a whole, the present results on the dHvA effect and FS in $TmGa_3$ and $ErGa_3$ at ambient pressure are in good agreement with the recent two-dimensional angular correlation of the positron annihilation radiation (2D-ACAR) studies (Refs. 9 and 10, respectively). The calculated pressure derivatives of the dHvA frequencies in $LuGa_3$ and $TmGa_3$ appeared to be in qualitative agreement with the experimental data, though the origin of some discrepancies found for $d\ln F/dP$ in $TmGa_3$ is not clear. The estimated magnetic contributions to the mass enhancement factor λ in $ErGa_3$ and $TmGa_3$ appeared to be large and magnetic field dependent. We admit that more work is needed to elucidate the nature of the large cyclotron masses observed in RGa_3 and, in particular, to evaluate the magnetic excitations effects on m_c^*. Also, the surprisingly large and highly anisotropic pressure effect on the cyclotron masses has been observed in $LuGa_3$ and especially in $TmGa_3$, which can not be explained within the employed standard rare-earth model. It has to be emphasized that different interactions (exchange splitting, CF and magnetic-quadrupolar excitations, spin waves) have to be taken into account in a further theoretical analysis of the revealed pressure effects on the FS and cyclotron masses in RGa_3. Also, at the present stage a more elaborated study is necessary to estimate the scale of the hybridization effects with $4f$ states in $ErGa_3$ and $TmGa_3$ within modern theoretical approaches (e.g. LSDA + U). These tasks apparently go beyond the aim of the present work, in which we tried to reach a true LSDA limit within the standard rare-earth model in order to explain the experimental dHvA data. It can be also beneficial to supplement such theoretical efforts with the experimental study of the pressure effect on the dHvA frequencies and cyclotron masses in the relative RIn_3 compounds.

The authors dedicate this work to the 90th anniversary of E.S. Borovik, who was one of pioneers of the Fermi surfaces studies [34].

We are grateful to Professors J. Klamut, T. Palewski, V. Nizhankovskii, and I.V. Svechkarev for their kind support and fruitful scientific discussions.

This work has been partly supported by The Swedish Natural Science Research Council (VR) and The Swedish Foundation for Strategic Research (SSF).

1. V.B. Pluzhnikov, A. Czopnik, and I.V. Svechkarev, *Physica* **B212**, 375 (1995).
2. V.B. Pluzhnikov, A. Czopnik, G.E. Grechnev, N.V. Savchenko, and W. Suski, *Phys. Rev.* **B59**, 7893 (1999).

3. V.B. Pluzhnikov, A. Czopnik, and G.E. Grechnev, *J. Phys.: Cond. Matter* **11**, 4507 (1999).
4. V.B. Pluzhnikov, A. Czopnik, O. Eriksson, G.E. Grechnev, and Yu.V. Fomenko, *Fiz. Nizk. Temp.* **25**, 894 (1999) [*Low Temp. Phys.* **25**, 670 (1999)].
5. N. Nagai, I. Umehara, T. Ebihara, A. K. Albessard, H. Sugawara, T. Yamazaki, K. Satoh, and Y. Onuki, *Physica* **B186 — 188**, 139 (1993).
6. S. Nojiri, Y. Katayama, D. Aoki, N. Suzuki, K. Sugiyama, R. Settai, Y. Inada, Y. Onuki, and H. Harima, *Physica* **B281 — 282**, 747 (2000).
7. T. Ebihara, D. Aoki, Y. Inada, R. Settai, K. Sugiyama, Y. Haga, and Y. Onuki, *J. Magn. Magn. Mater.* **226 — 230**, 101 (2001).
8. M. Biasini, G. Ferro, and A. Czopnik, *Phys. Rev.* **B68**, 094513 (2003).
9. M. Biasini, G. Kontrym-Sznajd, M.A. Monge, M. Gemmi, A. Czopnik, and A. Jura, *Phys. Rev. Lett.* **86**, 4616 (2001).
10. M. Biasini, G. Ferro, G. Kontrym-Sznajd, and A. Czopnik, *Phys. Rev.* **B66**, 075126 (2002).
11. A. Czopnik, Cz. Bazan, N. Iliev, B. Stalinski, H. Madge, and R. Pott, *Physica B&C* **130**, 262 (1985).
12. P. Morin, M. Giraud, P. L. Regnault, E. Roudaut, and A. Czopnik, *J. Magn. Magn. Mater.* **66**, 345 (1987)
13. P. Morin, M. Giraud, P. Burlet, and A. Czopnik, *J. Magn. Magn. Mater.* **68**, 107 (1987).
14. P. Morin, J. Rouchy, M. Giraud, and A. Czopnik, *J. Magn. Magn. Mater.* **67**, 95 (1987).
15. J. Pelleg, G. Kimmel, and D. Dayan, *J. Less—Common Met*. **81**, 33 (1981).
16. T.F. Smith, C.W. Chu, and M.B. Maple, *Cryogenics* **9**, 53 (1969).
17. A. Czopnik, A.S. Panfilov, and I.V. Svechkarev, *Fiz. Nizk. Temp.* **20**, 48 (1999) [*Low Temp. Phys.* **20**, 39 (1994)].
18. G.E. Grechnev, A.S. Panfilov, I.V. Svechkarev, K.H. J. Buschow, and A. Czopnik, *J. Alloys Compd.* **226**, 107 (1995).
19. M.S.S. Brooks and B. Johansson, in: *Ferromagnetic materials*, vol. **7**, K.H.J. Buschow (ed.), North—Holland, Amsterdam (1993), p. 139.
20. R. Ahuja, S. Auluck, B. Johansson, and M.S.S. Brooks, *Phys. Rev.* **B50**, 5147 (1994).
21. A.G. Petukhov, W.R.L. Lambrecht, and B. Segall, *Phys. Rev.* **B53**, 4324 (1996).
22. U. von Barth and L. Hedin, *J. Phys.* **C5**, 1629 (1972).
23. B.I. Min, H.J. F. Jansen, T. Oguchi, and A.J. Freeman, *J. Magn. Magn. Mater.* **61**, 139 (1986).
24. J.F. Herbst and J.W. Wilkins, in: *Handbook on the Physics and Chemistry of Rare Earths*, vol. **10**, K.A. Gschneidner, Jr, L. Eyring and S. Hufner (eds.), North— Holland, Amsterdam (1987), p. 321.
25. A.J. Freeman, B.I. Min, and M.R. Norman, in: *Handbook on the Physics and Chemistry of Rare Earths*, vol. **10**, K.A. Gschneidner, Jr, L. Eyring and S. Hufner (eds.), North—Holland, Amsterdam (1987), p. 165.
26. M.S.S. Brooks, L. Nordstrom, and B. Johansson, *Physica* **B172**, 95 (1991).
27. O. Eriksson and J.M. Wills, in: *Electronic Structure and Physical Properties of Solids*, Hugues Dreysse (ed.) Springer, Berlin (2000), p. 247.
28. G.E. Grechnev, A.S. Panfilov, I.V. Svechkarev, A. Delin, B. Johansson, J.M. Wills, and O. Eriksson, *J. Magn. Magn. Mater.* **192**, 137 (1999).
29. G. Lonzarich and A.V. Gold, *Can. J. Phys.* **52**, 694 (1974).
30. A. Murasik, A. Czopnik, L. Keller, and P. Fischer, *J. Magn. Magn. Mater.* **213**, 101 (2000).
31. P. Fulde and M. Loewenhaupt, *Adv. Phys.* **34,** 589 (1986).
32. R.M. White and P. Fulde, *Phys. Rev. Lett.* **47**, 1540 (1981).
33. P. Fulde and J. Jensen, *Phys. Rev.* **B27**, 4085 (1983).
34. E.S. Borovik, V.G. Volotskaya, and N.Ya. Fogel, *Zh. Eksp. Teor. Fiz.* **45**, 46 (1963) [*Sov. Phys. JETP* **18**, 34 (1963)]; E.S. Borovik and V.G. Volotskaya, *Zh. Eksp. Teor. Fiz.* **48**, 1554 (1965) [*Sov. Phys. JETP* **21**, 1041 (1965)].